Parallel transmission in a synthetic nerve

Charlotte E.G Hoskin[1,2,4], Vanessa Restrepo Schild[1,4], Javier Vinals Camallonga[3], Hagan Bayley[1*]

[1] *Department of Chemistry, University of Oxford, Oxford, UK*
[2] *Synthetic Biology Centre for Doctoral Training, University of Oxford, Oxford, UK*
[3] *Department of Biochemistry, University of Oxford, Oxford, UK*
[4] *Contributed equally to this work*
* *Corresponding author*

Abstract

Bioelectronic devices that are tetherless and soft are at the frontline of developments in medicine, robotics, and chemical computing. Here, we describe bioinspired synthetic neurons, composed entirely of soft, flexible biomaterials, capable of rapid electrochemical signal transmission over centimetre distances. Like natural cells, our synthetic neurons release neurotransmitters from their terminals which initiate downstream reactions. The components of the neurons are nanolitre aqueous droplets and hydrogel fibres, connected through lipid bilayers. Transmission is powered at upstream bilayers by light-driven pumps and mediated by ion-conducting protein pores. By bundling multiple neurons into a synthetic nerve, we show that distinct signals can propagate simultaneously along parallel axons, thereby transmitting spatiotemporal information. Synthetic nerves might play roles in next-generation implants, soft machines, and computing-devices.

Introduction

The emerging field of bioelectronics focuses primarily on the development of implantable and wearable medical devices that modulate the bioelectrical activity of target tissues to produce therapeutic effects[1-5]. Similar technologies are accelerating progress in robotics[6,7] and computing-devices[8-12]. However, hampered by their stiff electrodes, traditional devices are yet to reach their full potential. Such electrodes often degrade over time resulting in loss of communication with living cells. Further, the stiff electrode materials, e.g., metals, create a poor device-tissue interface leading to indiscriminate targeting of cells, and tissue damage[3]. Efforts to address these limitations have involved encapsulating the electrodes with soft or biological components[13,14] or have focused on electrode miniaturisation and improved flexibility[4,13]. Yet such modifications are unable to alter the inherent mechanical properties of these materials, meaning they remain too stiff to meet the mechanical requirements of living tissues[3].

Mechanical properties are not the only issue faced by bioelectronics. Conventional electrodes are limited to the use of electrical impulses (fields and currents) as signals for detection by living cells[2,4]. However, in cell communication signalling is largely based on the release of ions and molecules[15,16]. Progress has been made by replacing conventional electrodes in devices with soft electrode materials, such as conducting polymers[17-20]. With improved biocompatibility and pliability, devices built from such materials address many of the inherent limitations of conventional technologies. For instance, soft electrode materials have been used to mediate ionic signalling and thereby offer enhanced interfaces with tissues[20-22], but so far approaches have been

limited to the diffusion of electrolytes from the electrodes to living cells. Moreover, not only are conducting polymers limited with respect to what they can release but also by the requirement for connection to rigid external hardware for power or signal amplification[17,21]. Nonetheless such materials have been shown function at the abiotic-biotic interface[5,12,20], as they are able to communicate with living tissues, paving the way for novel devices for both therapeutics and diagnostics.

Droplet networks are another class of soft material which have shown promise as they can be patterned with discrete compartments encapsulating various ions and molecules[23-28]. In addition, the droplet interface bilayers can be functionalised with membrane proteins, such as pores[23-25,28] and pumps[25,26], enabling communication. Previous work, employing droplet networks, has demonstrated simple signal transduction by either ionic[23-26] or chemical[27,28] signals. But despite the potential utility of these materials in soft bioelectronics, future devices would benefit from tetherless powering, removing the need for stiff, bio-incompatible components.

Here, we describe the fabrication of a synthetic nerve: a wireless, bioinspired device composed entirely of soft materials. Remotely powered by light, the synthetic nerve (Fig. 1) is a cable-like bundle of axons that conveys sensory information over centimetre distances. Our design differs from previous (bilayer-based) communicating networks[23-25,27] in that each of our synthetic axons is one continuous hydrogel. In addition, the bioinspired device uses both ionic and molecular signals for communication[15,16] (Fig 2-4). Each synthetic nerve contains a 3-dimensional arrangement of seven parallel signalling pathways, comprising nanolitre aqueous droplets and hydrogel fibres connected via lipid bilayers (Fig. 1). Through stimuli and droplet patterning, rapid and directional signalling can be achieved with spatiotemporal resolution (Fig. 4); albeit using a non-biomimetic transmission mechanism (Fig. S1, S2). We believe that the external activation of light-driven proteins to propagate sensory information is a significant step towards the development of tetherless bioelectronics for applications at the abiotic-biotic interface, in neurorobotics, neuro-prosthetics and computing.

Results

Design of bioinspired synthetic neurons and nerves

Neurobiological architectures and functions inspired the design of our synthetic neurons and nerves. Constructed by using soft biological materials, the synthetic neurons and nerves employ communication principles found in nature: the conduction of ions and the translocation of molecules, albeit by using different mechanisms[15,16] (Fig. 1b, S1, S2).

Critical to our synthetic neurons is the photochemistry of archaerhodopsin-3 (aR3), a light-driven (hydrogen ion, H^+) pump found within the claret membrane (CM) patches of *Halorubrum sodomense*[29] (Fig. S3). Aqueous droplets (200 nL) containing CM-aR3 (henceforth referred to as sensory droplets, Fig. 1c, pink, ‘1’) were interfaced with a synthetic axon (Fig. 1c, blue, ‘2’) forming a sensory lipid bilayer into which CM-aR3 inserted vectorially. The axon of our initial synthetic neuron design was composed of a series of aqueous droplets connected through droplet interface bilayers (DIBs),

resembling those previously used in the literature[23-25,28]. But in our final design, long axons were formed from an ionotronic hydrogel[18,19] (agarose containing mobile ions) to afford structural stability and flexibility whilst maintaining low resistance (Fig. 1c-d). The longest axons built (25 mm) were comparable in length to those of the human optic nerve[38] (Fig. 1c). In addition, they had similar diameters (0.7 – 1.0 mm) to those found in nature, albeit at the upper end; the squid giant axon (*Architeuthis dux*) is 0.5 – 1.5 mm wide[15]. At the other end of the synthetic axon were two additional aqueous droplets (200 nL): the presynaptic (green, '3') and postsynaptic (yellow, '4') droplets (Fig. 1c, 3). The presynaptic droplet contained the pore-forming protein α-hemolysin (αHL), and the small molecule neurotransmitter ATP (or the fluorescent analogue, MANT-dATP). This droplet formed one bilayer with the synthetic axon and another (the synaptic bilayer) with the postsynaptic droplet (Fig. 1c).

In nature, neurons are assembled into fascicles, which may combine to form larger nerve bundles[3,15] (Fig. 1a). In the present work, we also fabricated a small synthetic nerve bundle (a single fascicle), enclosing seven hydrogel-based neurons within a synthetic elastomeric polymer (Sylgard 184)[3] which protected and electrically insulated the synthetic axons (Fig. 1d, 4). All our synthetic nerves functioned in the absence of tethers, requiring only light for power.

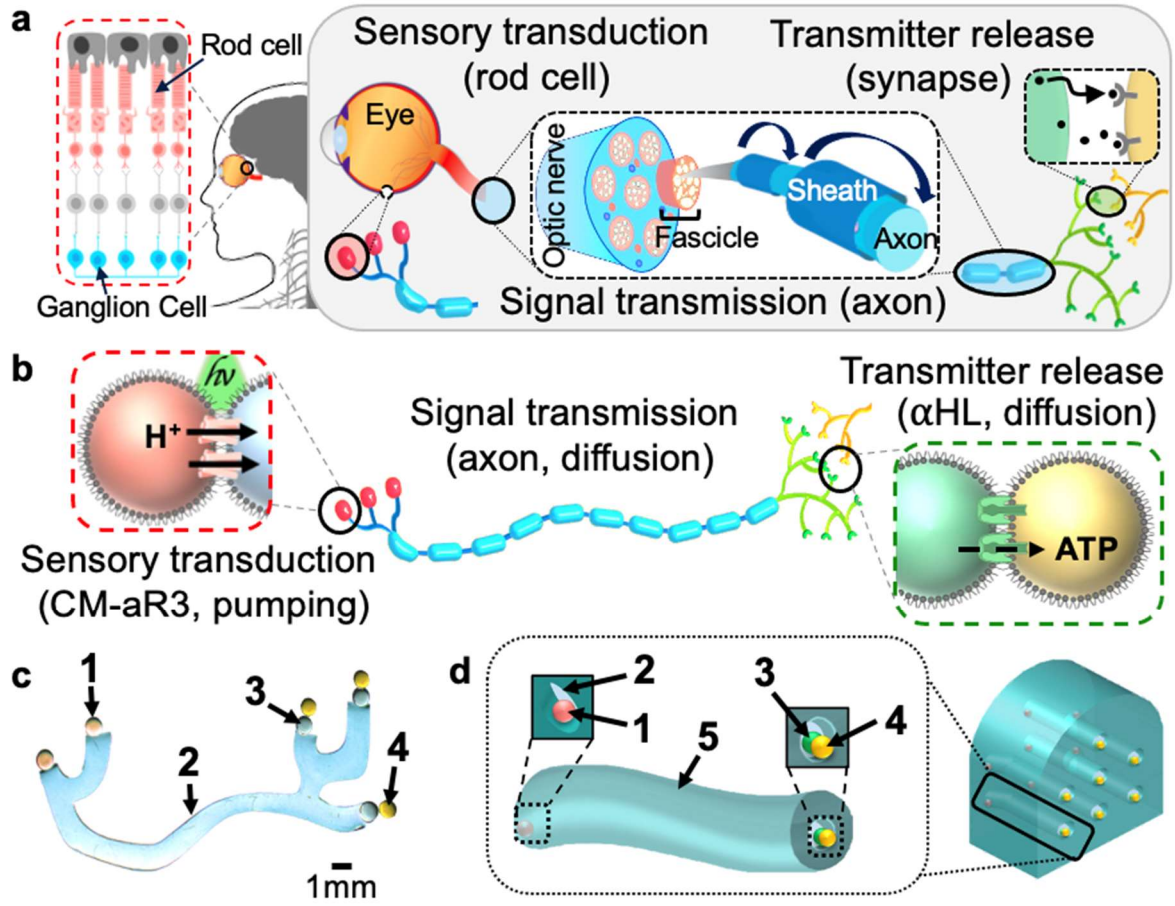

Fig. 1 | Design of a bio-inspired synthetic nerve. a, Schematic of a natural nerve. Rod cells (in the eye, pink) transduce light into ionic signals and, in concert with bipolar (light grey) and ganglion (blue) cells, relay sensory information to the brain (as an action potential). Inter-cell communication is via neurotransmission at synapses. At the back of the eye, ganglion cells are myelinated and bundle into fascicles. The optic nerve is composed of multiple fascicles. **b,** Schematic of a synthetic neuron. CM-aR3 transduces a light stimulus ($h\nu$, green) into an ionic signal, by electrogenically pumping H^+ ions across the sensory bilayer (red box). Signal transmission occurs by the spreading of this positive charge throughout the neuron. This occurs through the flux of ions through αHL pores located in the axon and synaptic bilayers. Charge neutralisation then occurs by the movement of negatively charged ions and molecules. Accordingly, at the synaptic terminals the neurotransmitter (ATP^{4-}) is directionally released by moving through αHL pores in the synaptic bilayer (green box) (see 'Supplementary Information'). **c,** Photograph (background removed, see 'Materials and Methods', Fig. S29) of a synthetic neuron. Coloured dyes were included for visualisation: sensory droplet ('1', pink), axon ('2', blue), presynaptic droplet ('3', green), postsynaptic droplet ('4', yellow). **d,** Design of an insulated synthetic neuron and a synthetic nerve. Neuron: an insulating elastomer sheath ('5', teal) surrounds the hydrogel axon ('3', blue). At one end of the axon was the sensory droplet ('1', pink) and at the other end were the presynaptic and postsynaptic droplets ('3', green and '4', yellow respectively). Nerve: a synthetic nerve bundle containing seven neurons.

Rapid sensory transduction by CM-aR3

In the human eye, rod cells contain rhodopsin proteins which detect low light levels, initiating a cascade of events that conveys sensory information to the brain[15] (Fig. 1a). Microbial rhodopsins are simple, electrogenic proteins, which are structurally comparable with human rhodopsins[29-31]. The incorporation of microbial rhodopsins into our synthetic neuron enabled light to generate ionic signals (via H^+ pumping) within the device in a tetherless manner (Fig. 2-4).

Sensory receptors of the synthetic neurons contained CM-aR3 (CM fragments obtained by expression in *H. sodomense*), which generate larger signals than other known microbial (H^+) pumps[29], perhaps due to its faster photocycle[30,34] or to more efficient incorporation into membranes. A CM-aR3-containing aqueous droplet (200 nL, 100 mM MES, 100 mM NaCl, 0.001% DDM (w/v), 0.15 – 0.25 mg mL^{-1} CM-aR3, pH 6.5) was encapsulated in a lipid monolayer after it was formed by pipetting into a lipid-in-oil solution (hexadecane and silicone oil (35:65 (v/v)) containing 1,2-diphytanoyl-sn-glycero-phosphatidylcholine (DPhPC, 10 mg mL^{-1})). By bringing a protein-free aqueous droplet (axon droplet, A), formed in the same manner, into contact with the CM-aR3 sensory droplet (S), a DIB was formed into which the protein inserted (Fig. 2a, S4). The inclusion of MES buffer in the droplets prolonged the time before CM-aR3 activity was hindered by the build-up of a pH gradient[35,36].

When illuminated, the photochemically-driven CM-aR3 proteins pumped H^+ ions across the membrane, producing ionic signals. To characterise these sensory DIBs, responses to light were measured with Ag/AgCl electrodes (Fig. 2a); the tethers were not required for function. When activated with yellow-green light (YG, 490 – 608 nm with peaks at 560 nm and 592 nm, 15 $\pm$ 4.5 mW) we observed signals of >2.0 pA across the DIB, which we set as an arbitrary threshold to indicate protein activity (Fig. 2c, S4-6). The average steady-state signal recorded across the sensory bilayer was +19 $\pm$ 3.9 pA (mean $\pm$ SD, n = 10 DIBs, Fig. 2c); the maximum was +25 pA. The signals were maintained upon prolonged (1h) illumination (YG light) and were repeated during a series of light pulses (YG light, 30s on, 0.01ȯ Hz, Fig. S7). The rapid photocycle of CM-aR3[30,34] enabled signals to be repeated following brief stimulation (YG light, 20 ms on, 0.0ȯ Hz) (Fig. 2d), analogous to the firing of successive action potentials along natural neurons[37]. Based on the current signals, we calculated that 10^5 - 10^6 functional CM-aR3 proteins vectorially insert into a DIB (see SI 'Theoretical considerations').

Whilst there was variation in the signal magnitude, both within a single protein batch and between expression batches, the signal polarity was consistent (Fig. S8). In 100 consecutive experiments (using protein from 13 different batches prepared following the same protocol), we observed that CM-aR3 always inserted into DIBs predominantly N-terminus first (Fig. S8), as previously seen with the microbial pump bR[25,26], generating positive signals upon illumination. A positive signal is defined as one in which electrons flow towards the ground electrode in the external circuit (see Materials and Methods). Therefore, hydrogen ions must move out of the sensory droplet, which contains the recording electrode, into the axon droplet, which is at ground (Fig. 2a). Further, negative signals were generated following the addition of CM-aR3 to the ground electrode-containing droplet, instead of recording-electrode containing droplet (Fig. S8). We also performed control experiments in the absence of

protein (NP); no signals were generated, confirming that there were no artefacts occurring from photochemistry at the Ag/AgCl electrodes under our conditions (Fig. 2b, S8).

In addition, sensory transduction was observed in an electrode-free manner by the addition of the pH-sensitive fluorophore pyranine into the sensory and axon droplets (in the absence of buffer) (Fig. S9). A calibration curve relating the fluorescence intensity to pH was constructed (Fig. S10, 100 μM; pK_a = 7.3), from which H^+ movement across the sensory bilayer was quantified[36] (Fig. 2e, S9, S10). Following overnight illumination (YG light, 15 h), we observed an increase in pH of the CM-aR3 sensory droplet of +0.3 ± 0.0 pH units, and a decrease of -0.5 ± 0.0 pH units in the (protein-free) axon droplet (mean ± SD, n = 3 DIBs, Fig. 2e). These pH changes match both calculations of the extent and direction of CM-aR3 insertion (as determined from electrical recordings, see SI: 'Theoretical considerations'), and the reported CM-aR3 photocycle rate[34].

Directional signal transmission along centimetre-long synthetic axons

The synthetic neurons transmitted ionic signals directionally along artificial axons; the longest characterised here were 25 mm in length (Fig. 2e, S11, S12). By comparison, a human optic nerve is approximately 30 mm long[38]. For our synthetic axons, we explored the use of a chain of aqueous droplets (resembling those previously used in the literature[22-24,27]) before opting for a continuous hydrogel fibre (Fig. 1c) which enabled greater signal transmission, due to its lower resistance (Fig. S12).

For droplet-based axons, a series of 200 nL aqueous droplets (~700 μm diameter), connected through DIBs, was used (Fig. S11). The sensory bilayer, described above, was composed of a DIB formed between a CM-aR3-containing sensory droplet (S, 0.15 - 0.25 mg mL^{-1} CM-aR3) and a protein-free axon droplet. All downstream droplets in the axon contained the pore-forming protein αHL (50 nM monomeric αHL). Ag/AgCl electrodes were used to record signal transmission along axons of increasing length; the ground electrode was inserted into the terminal droplet of the axon chain. By including additional droplets, and therefore additional DIBs, in the extended axon, the overall resistance was expected to increase, reducing the signal transmitted at a fixed applied potential (here 0 mV). Indeed, as the length of the synthetic neuron was increased from 2 to 15 droplets, the signal decreased by more than 70% from +22 ± 1.3 pA to +4.4 ± 0.1 pA (mean ± SD, n = 3 independent neurons, Fig. S11). The longest (15-droplet) synthetic neuron tested was ~10-mm in length and produced directional signal transmission (> 2.0-pA threshold).

Hydrogen ion movement in the synthetic axon was quantified with the pH-sensitive fluorophore pyranine (in the absence of buffer) (pK_a = 7.3, fluorescence increases with pH, Fig. S10, S11)[36]. Illumination of a tetherless 5-droplet synthetic neuron (YG, 15 ± 4.5 mW, 15 h) resulted in the sensory droplet (S) pH increasing by +0.2 ± 0.1 pH units (mean ± SD, n = 3 independent neurons, Fig. S11). All other droplets decreased in pH, as observed by a reduction in fluorescence intensity, upon illumination. The pH of the terminal presynaptic droplet (pre) decreased by -0.2 ± 0.0 pH units (mean ± SD, n = 3 independent neurons), demonstrating signal transmission along the entire axon in the absence of electrical tethers.

We also examined synthetic axons formed from a continuous hydrogel polymer (Fig. 2e, S12). Capacitance measurements indicated that bilayers formed between a droplet and hydrogel (DHBs) were larger in area than those formed between two droplets (DIBs) (Fig. S13). This allowed more CM-aR3 to insert into the bilayer and consequently generate larger ionic signals and pH changes. First, we inserted Ag/AgCl electrodes into aqueous droplets (200 nL) at each end of the hydrogel axon to enable signal detection. The recording electrode was in the CM-aR3 sensory droplet (S) and the ground electrode was in the presynaptic droplet (Pre, 50 nM monomeric αHL). Increasing the hydrogel axon length from 0 to 10 mm resulted in a decrease in signal from +22 $\pm$ 1.3 pA to +10 $\pm$ 1.0 pA (mean $\pm$ SD, n = 3 independent neurons) (Fig. S12). A greater ionic signal was transmitted over a 10-mm distance than by its droplet counterpart. Since there were only two DHBs in the conducting pathway of the hydrogel neuron, the overall resistance was reduced compared to the combined resistance of the series of DIBs in the droplet neuron (Fig. S12). We then built a synthetic neuron with a 25-mm long hydrogel axon (Fig. 2e, S12) to test whether signals could be transmitted over biologically relevant distances[38], and indeed a signal of +7.3 $\pm$ 1.5 pA (mean $\pm$ SD, n = 3 independent neurons) was detected (Fig. S12).

Optical monitoring with pyranine showed that upon illumination hydrogen ions were pumped out of the CM-aR3 sensory droplets (S, pink) and moved into the presynaptic droplets (Pre, blue, 50 nM αHL) located at the other end of the hydrogel axon[36]. The resulting changes in pH were calculated using droplet fluorescence and a calibration curve (Fig. S10). Sensory droplet pH increased by +0.4 $\pm$ 0.1 and presynaptic droplet decreased by -0.6 $\pm$ 0.1 pH (mean $\pm$ SD, n = 3 independent neurons, Fig. 2e, S12). Hydrogel-based axons also offered greater stability and flexibility and they can be made into almost any size or shape[19].

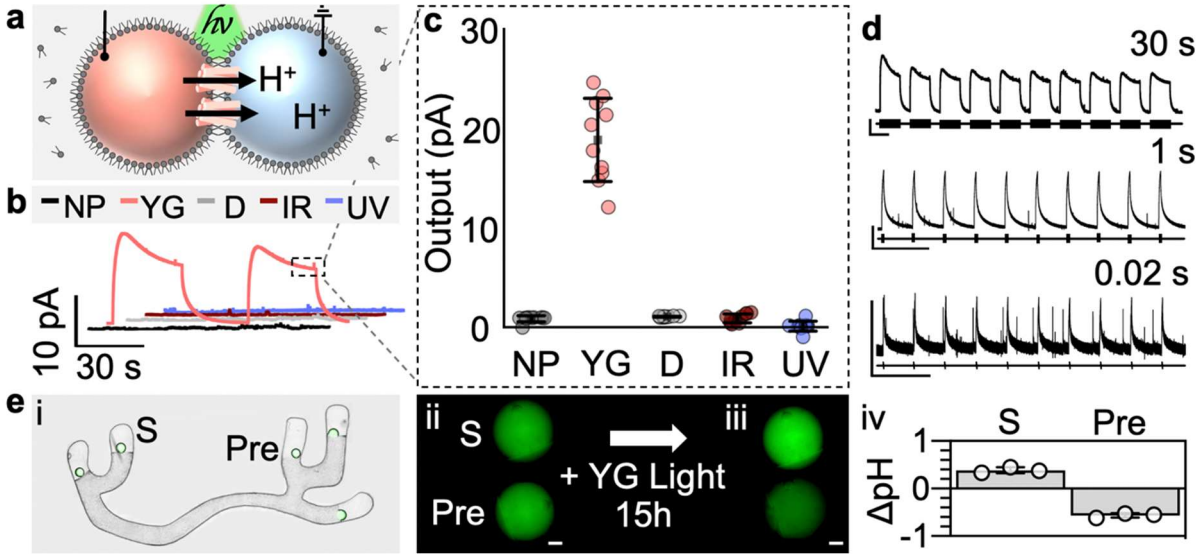

Fig. 2 | Rapid sensory transduction and directional transmission in a synthetic neuron. a, DIB showing H^+ ion movement upon CM-aR3 illumination (hν). Recording and ground electrodes were inserted into the sensory (pink) and axon (blue) droplets for signal recording. All droplets (200 nL) contained 100 mM NaCl, 100 mM MES, pH 6.5; sensory droplets also included 0.15 – 0.25 mg mL^{-1} CM-aR3 and 0.001% DDM (w/v). **b,** Signal recorded across the DIB with 2 light pulses (30 s, 0.01ȯ Hz). H^+ ions were pumped out of the sensory droplet (pink) upon illumination with YG light (peaks at 550 nm and 592 nm, 15 ± 4.5 mW). No signal output (below the 2.0-pA threshold) was recorded in the absence of protein (NP, black) or light (D, grey), nor when illumination was with IR (red, peak at 722 nm, 16 ± 5.0 mW) or UV (blue, peak at 376 nm, 15 ± 3.9 mW) light. Box outlines steady-state output. **c,** Steady-state output (mean ± SD, n = 10 independent DIBs). **d**, Effects of YG light pulses on a CM-aR3 DIB: 30 s pulses (top, 0.02̇ Hz), 1 s pulses (middle, 0.0ó Hz) and 0.02 s pulses (bottom, 0.0ó Hz). Black bars indicate light-on**. e,** i, Bright-field and fluorescence microscopy overlay of a tetherless hydrogel neuron: here sensory (S, with CM-aR3) and presynaptic (Pre, with 50 nM αHL) droplets contain 100 μM pyranine (in the absence of buffer). Overlapping images are stitched together (see Materials and Methods, Fig. S31). ii, iii Fluorescence microscopy images (minus background, see Materials and Methods, Fig. S30) of the sensory (S) and presynaptic (Pre) droplets before 'ii' and 'iii' after overnight illumination (15 h, YG light, fluorescence increases with pH). Scale bar = 200 μm**.** iv, Droplet pH change upon illumination (mean ± SD, n = 3 independent neurons) determined from the calibration curve (see Materials and Methods).

Light-powered electrochemical communication

Interneuronal communication occurs at synaptic junctions through the transmission of chemical or ionic signals[15,16]. Generally, synaptic communication is mediated by neurotransmitters, which are released when an action potential reaches the synapse[13,14] (Fig. 1a). Several substances may be simultaneously released from a single synapse: co-transmission[15,39]. As previously noted, our synapse-mimic is composed of two aqueous droplets connected via a lipid bilayer: the presynaptic (3, green) and postsynaptic (4, yellow) droplets (Fig. 1c, 3a). Presynaptic droplets contain αHL and a neurotransmitter.

We have already demonstrated that our tetherless synthetic neurons can release ionic neurotransmitters (e.g., hydrogen ions[40,41]) (Fig. 2, S11, S12). To mimic a small-molecule neurotransmitter, we used the fluorescent ATP analogue, MANT-dATP (Fig. S14). ATP is co-released at most neuronal synapses (as well as by associated glial cells), and has been shown to be involved in a diverse range of physiological actions[39,42].

In our experimental system (50 nM αHL, continuous illumination, tetherless 4-droplet neuron), spontaneous diffusion alone did not release a significant concentration of MANT-dATP (in either direction) (Fig. S15). By using a calibration curve (Fig. S14), we determined that the concentration of MANT-dATP transferred after 24 h in the dark was below the detection threshold (<18 μM, n = 3 independent synthetic neurons) (Fig. S15). To confirm that an electrical gradient could drive the directional movement of MANT-dATP, we used Ag/AgCl electrodes, with the recording electrode in the axon droplet and the ground electrode in the postsynaptic droplet. A negative potential (- 50 mV) was then continuously applied (for 1 h) and 44 $\pm$ 0.9 μM of MANT-dATP moved (via αHL pores) into the postsynaptic droplet (mean $\pm$ SD, n = 3 independent synthetic neurons) (Fig. S16).

As a first demonstration of photochemically powered neurotransmission, we built a short synthetic 4-droplet neuron (~2.8 mm, tetherless, Fig. S17). First, the synthetic neuron was illuminated, and hydrogen ions (H^+) were electrogenically pumped across the sensory bilayer (Fig. S17-19). This positive charge then spread throughout the neuron (using the αHL pores embedded within the bilayers); the charge was carried by positively charged ions (e.g., H^+, Na^+). Next, the positive charge of the axon, presynaptic and postsynaptic droplets (Fig. S17-19) was then slowly neutralised by the movement negatively charged ions (e.g., Cl^-) which moved down the neuron from the sensory to the synaptic terminal. Accordingly, the negatively charged MANT-dATP neurotransmitters (MANT-dATP^{4-}) also moved, directionally, into the postsynaptic droplet. Upon overnight stimulation (YG light, 15 h) 35 $\pm$ 1.4 μM of the MANT-dATP neurotransmitter moved across the synaptic bilayer (mean $\pm$ SD, n = 3 independent neurons) (Fig. S14, S17). We then built a long synthetic hydrogel neuron (25 mm, tetherless) and, following prolonged stimulation (YG light, 15 h), 28 $\pm$ 2.6 μM MANT-dATP moved across the synaptic bilayer (mean $\pm$ SD, n = 3 independent neurons) (Fig. 3a-d, S14, S19).

Imitating the electrochemical communication of a biological afferent neuron, albeit using a different mechanism, our tetherless synthetic neurons used a combination of ionic and chemical signals to convey sensory information. In nature, neurotransmitters

are packaged into vesicles and released into the synaptic cleft[15,16]. However, transmission from our tetherless synthetic neurons was by movement through αHL pores, down an electrochemical gradient (Fig. 3b-d, S17-19). For now, the absence of transmitter synthesis or re-uptake machinery within our synthetic neurons means that neurotransmitter availability is finite[15,16].

Downstream signalling in a synthetic neuron

In nature, neurotransmitter release initiates a response downstream[15,16]. Mimicking this process, we used the ATP transferred by our synthetic neurons in a downstream enzymatic reaction, in which glycerol is phosphorylated and then oxidised to a glycolytic intermediate. Hydrogen peroxide produced in this process then generated fluorescent resorufin in another enzymatic conversion (Fig. 3e).

First, we built and illuminated (YG light, 15 $\pm$ 4.5 mW, 15 h) a short synthetic droplet neuron (4 droplets, tetherless, 200 nL, ~2.8 mm total length, Fig. S20). Here, the presynaptic droplet contained ATP and monomeric αHL. After neurotransmitter (ATP) release, a neighbouring droplet (200 nL, Fig. 3b, 'N') was pipetted at the synaptic terminal of the synthetic neuron (see Materials and Methods). This neighbouring droplet ('N') contained the precursors and enzymes required for the ATP-dependent downstream reaction. Next, the postsynaptic droplet (Fig. 3b, '4') was mechanically separated from the presynaptic droplet by using a silver wire, (Fig. 3b, '3'), before fusion with the neighbouring droplet (Fig. 3b, 'N'). Separation was required to prevent droplet coalescence because the glycerol present in the neighbouring droplet increased droplet instability. The fused droplets (now 400 nL, '4+N') were incubated in the dark for 0.5 h to allow the ATP-initiated reactions to occur. The synthetic neuron was then regenerated by gently reconnecting the fused droplets to the presynaptic droplet (by gently tipping the chamber, Fig. 3e) and the resorufin produced was visualised by epifluorescence imaging (Fig. S20). A fluorescence output of 1280 $\pm$ 104 was generated after 0.5 h (mean $\pm$ SD, n = 3 independent neurons). Additionally, illumination of a long synthetic hydrogel neuron (25 mm, tetherless) produced a fluorescence output of 963 $\pm$ 28 (mean $\pm$ SD, n = 3 independent neurons, imaged 0.5 h after droplet fusion, Fig. S21). No fluorescence output was observed when the synthetic neuron was not illuminated (Fig. S21).

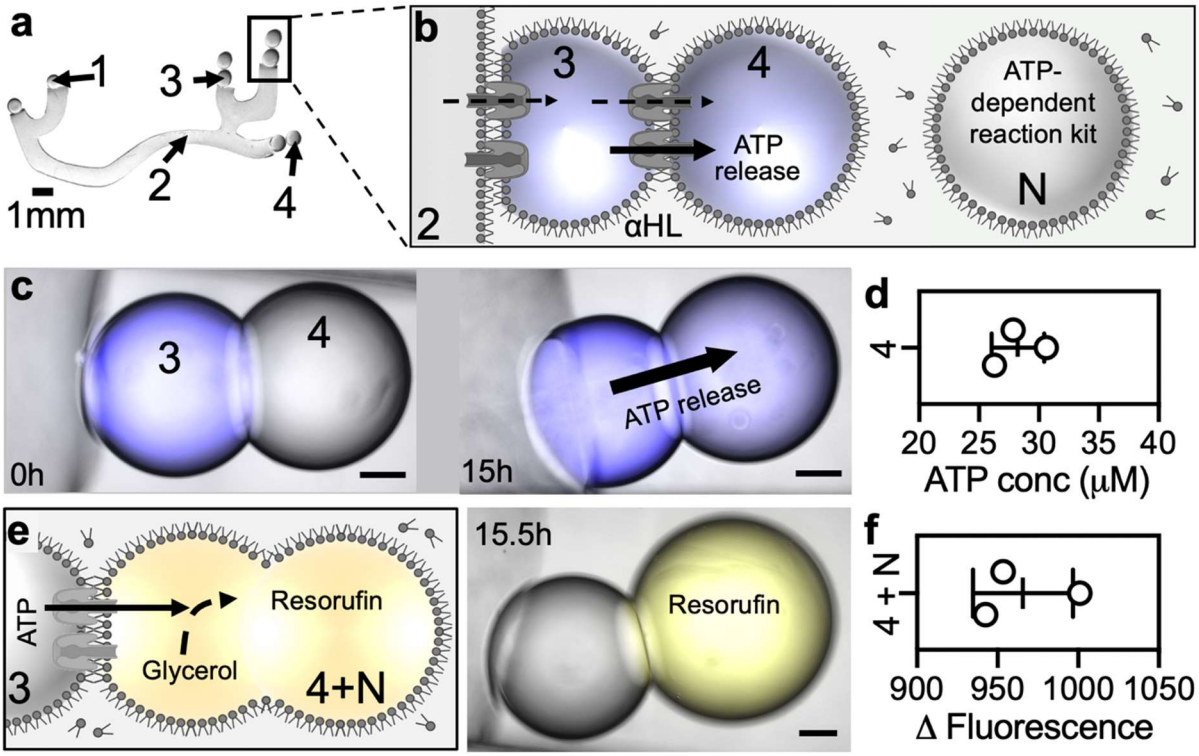

Fig. 3 | Electrochemical communication in a synthetic neuron. a, Photograph (background removed) of a synthetic (tetherless) hydrogel neuron. All elements contain 100 mM MES, 100 mM NaCl, pH 6.5. Additionally, sensory droplets ('1') contain CM-aR3 (0.15 – 0.25 mg mL^{-1}) and 0.001% DDM (w/v); the hydrogel axon ('2') contains 2% agarose; and presynaptic droplets ('3') contain αHL (50 nM) and 100 μM neurotransmitter (MANT-dATP or ATP). A synthetic synapse composed of presynaptic ('3') and postsynaptic ('4') droplets is boxed. Scale bar = 1 mm. **b,** Schematic of a synthetic synapse. Upon irradiation, H^+ ions are pumped electrogenically into the synthetic axon ('2'). The positive charge then spreads throughout the neuron, by using the αHL pores at the interfaces, moving into the presynaptic ('3') and then postsynaptic ('4') droplets through αHL pores. The positive charge is then slowly neutralised by the movement of negative ions and molecules, including the directional movement of the neurotransmitter ($MANT\text{-}dATP^{4-}$ or ATP^{4-}) into the postsynaptic droplet ('4'). Neighbouring droplets ('N') contain the materials required for the downstream ATP-dependent reactions. **c,** Brightfield, and fluorescence microscopy overlays of a synthetic synapse (see Materials and Methods, stitched image, Fig. S30, S31) before (0 h) and after (15 h) illumination (YG light, 15 ± 4.5 mW). Presynaptic droplets ('3') contain MANT-dATP, which moves into the postsynaptic droplets ('4'). Scale bar = 100 μm. **d,** MANT-dATP concentration in the postsynaptic droplets ('4') after illumination (as determined from a calibration curve, Fig. S14). **e,** Schematic (left) and stitched microscopy overlay (right) of the synaptic terminal after downstream signalling. Postsynaptic droplets ('4', 200 nL) and neighbouring droplets ('N', 200 nL) were mechanically fused ('4+N', 400 nL, using a Ag wire). ATP released into the postsynaptic droplet initiates the ATP-dependent reactions which produce fluorescent resorufin (after 0.5 h). Scale bar = 100 μm. **f,** Change in fluorescence as the result of resorufin formation in the fused droplets ('4+N').

An insulated synthetic neuron

Many natural neurons are surrounded with an insulating sheath (Fig. 1a, S1) which protects them from other electrical impulses and increases the rate of axon signal transmission[15]. We mimicked the protective properties of this sheath, without compromising synthetic neuron flexibility, by encasing the synthetic hydrogel axon in an elastomeric coat (Sylgard-184) (Fig. 1d, S22). Ag/AgCl electrodes were positioned in the droplets at either end of the axon to measure signal transmission. Upon illumination (YG light, 15 $\pm$ 4.5 mW) the 10-mm central axon of an insulated synthetic neuron conducted a signal of +14 $\pm$ 0.5 pA (mean $\pm$ SD, n = 3 independent neurons). However, no signal transmission occurred when the ground electrode was transferred to the elastomer from the presynaptic droplet (with the recording electrode remaining in the CM-aR3 sensory droplet): +0.2 $\pm$ 0.3 pA (below the 2.0-pA threshold, mean $\pm$ SD, n = 3 independent neurons, Fig. S23).

Parallel transmission of signals within a synthetic nerve bundle

In nature, parallel axons are bundled together and enclosed in a tubular layer of connective tissue forming nerve fascicles. Assemblies of fascicles form larger nerves (Fig. 1a)[3,15]. Individual axons are electrically isolated from each other to ensure that the signal transmitted along one neuron does not merge with those of neighbouring cells. Here, we fabricated a small synthetic nerve bundle (a single fascicle) containing seven (hydrogel) axons and demonstrated parallel signal transmission along three of the axons (Fig. 1d, 4, S24-26). There should be no crosstalk between the synthetic axons since the surrounding elastomer is an electrical insulator (Fig. S23). We tested two aspects of parallel signalling: stimulation of light pulses at three different frequencies (Fig. S25) and the use of three different photosensory proteins to initiate signalling (Fig. S26).

First, we built a (tethered) synthetic nerve in which three 10-mm hydrogel axons could be separately stimulated (with YG light, 0 mV applied potential) and the outputs individually measured (Fig. S25, see Methods and Materials). To demonstrate that the axons within our synthetic nerve could conduct distinct electrical signals, we stimulated each axon with a different light pattern: pulses of YG light with durations of 15 s, 5 s, and 1 s (at 0.05, 0.1 and 0.06 Hz, respectively). Using Ag/AgCl electrodes, we simultaneously recorded the three distinct signals that were conducted along the parallel axons of our synthetic nerve. The signals mirrored the stimulatory light patterns, thereby transmitting spatiotemporal information (Fig. 4c n1-3, S25).

Since our synthetic nerves functioned in the absence of tethers, requiring only light for power, we then demonstrated parallel transmission in a wireless synthetic nerve. We incorporated three different microbial rhodopsins[30] within the sensory droplets so that illumination with the same stimulus (YG light) produced different outputs (Fig. 4d, S26). We used the light-driven pumps CM-aR3[29,34] (as used in the rest of this work), bacteriorhodopsin (bR, from the purple membrane (PM) of *Halobacterium salinarum*) and *E. coli*-expressed aR3 (EC-aR3, the same protein sequence as CM-aR3 but with a C-terminal His-tag not in the CM-aR3) (Fig. S3, S26-27).

Before constructing the tetherless synthetic nerve, we first characterised these light-driven signals by placing Ag/AgCl electrodes on each side of the sensory bilayer (Fig.

2a, recording electrode in the sensory droplet). Upon illumination (YG light, 15 ± 4.5 mW), CM-aR3 and PM-bR sensory droplets generated positive signals (i.e., H^+ ions flowed out of the recording electrode-containing sensory droplets)[25,26]. By contrast, EC-aR3 generated negative signals upon illumination (i.e., H^+ ions flowed into the recording electrode-containing sensory droplets) (Fig. S27). EC-aR3 must insert into the DPhPC bilayer in the opposite orientation to CM-aR3, perhaps due to its monomeric state (confirmed by a shift in absorption[31]), non-native lipid composition (due to lack of CM)[33], the absence of the bacterioruberin carotenoid (found in the CM[43]) or the presence of a His-tag (see Materials and Methods). All sensory DIBs generated signal outputs above the 2.0-pA threshold with CM-aR3 producing larger signals than PM-bR and EC-aR3: +20 ± 3.7 pA, +6.9 ± 2.2 pA and -6.1 ± 1.4 pA respectively (mean ± SD, n = 10 independent DIBs, Fig. S27).

Next, we built the tetherless synthetic nerve; we added pyranine to all the sensory and presynaptic droplets (in the absence of buffer) (Fig. 4d, S26). For simplicity, we only patterned the three bottom 10-mm hydrogel axons (of the seven available, Fig. 4b). Upon illumination (YG light, 15 h), the pH of the sensory droplets (S, 100 mM NaCl, 100 μM pyranine, 0.001% DDM (w/v), 0.2 mg mL^{-1} rhodopsin), increased in the cases of CM-aR3 (n1) and PM-bR (n3), by +0.4 ± 0.0 and +0.1 ± 0.0 pH respectively, and decreased in the case of EC-aR3 (n2) by -0.1 ± 0.0 pH (mean ± SD, n = 3 independent synthetic nerves) (Fig. 4d, S10, S26). In the presynaptic droplets (Pre, 100 mM NaCl, 100 μM pyranine, 50 nM αHL), at the downstream end of the hydrogel axons, we observed an inverse pattern (Fig. 4d). For the CM-aR3 (n1) and PM-bR-containing (n3) synthetic neurons, the presynaptic droplet pH decreased by -0.4 ± 0.0 and -0.1 ± 0.0 pH respectively, while the pH in the synaptic droplet of EC-aR3 (n2) synthetic neuron increased by +0.1 ± 0.0 pH (mean ± SD, n = 3 independent synthetic nerves) (Fig. 4d, S10, S26).

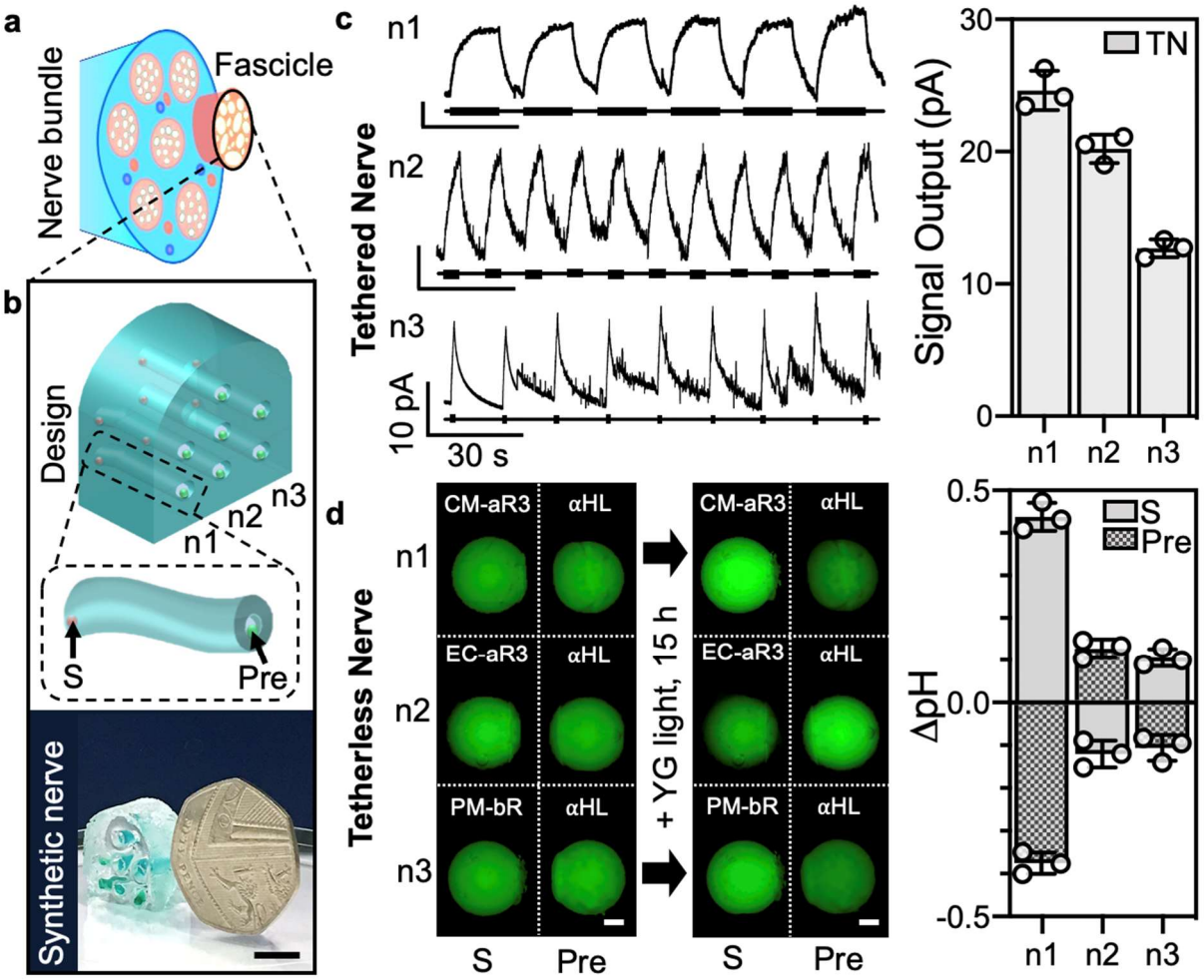

Fig. 4| Parallel transmission in a synthetic nerve. a, A natural nerve bundle containing several fascicles. **b,** *Top*: Design of a small synthetic nerve composed of one fascicle with seven hydrogel axons encased within an insulating elastomer sheath. The three conducting pathways that will be stimulated are labelled (n1, n2, n3). The zoom-in shows an elastomer-encased synthetic hydrogel axon with a sensory droplet (S, containing the proton pump) and presynaptic droplet (Pre, with αHL). *Bottom:* photograph of the synthetic nerve (in air) next to a 50 pence coin. Scale bar = 10 mm. **c,** A tethered synthetic nerve (TN) in which Ag/AgCl electrodes (in the terminal droplets) enabled signal detection; recording electrodes were placed in the sensory droplets and a common ground electrode in the presynaptic droplets. *Left:* Signals were recorded in the neurons (n1-3) following stimulation with different YG light pulses (15 s (0.05 Hz), 5 s (0.1 Hz) and 1 s (0.06 Hz), respectively, 15 ± 4.5 mW). *Right:* Steady-state signal output (n = 3 independent synthetic nerves, mean ± SD). **d**, A tetherless (electrode-free) synthetic nerve. The sensory droplets (S, 100 μM pyranine, 100 mM NaCl, 0.001% DDM (w/v), 0.15 - 0.25 mg mL^{-1} protein, pH 6.5) contained different proton pumps: n1, CM-aR3; n2, EC-aR3; n3, PM-bR. All presynaptic droplets (Pre) contained 100 μM pyranine, 100 mM NaCl, 50 nM αHL, pH 6.5. *Left:* Epifluorescence microscopy images (minus background, see Materials and Methods, Fig. S30) of the droplets before and after illumination (15 h, YG light). *Right:* Change in sensory (S, grey) and presynaptic (Pre, grey checked) droplet pH following illumination (n = 3 independent synthetic nerves). pH values were determined from a calibration curve (Fig. S10).

Outlook

Using nature as inspiration, and natural materials, we have developed a soft bioelectronic neural device, wirelessly powered by light (Fig. 2). Soft polymers and biologically compliant materials replace the constituents of comparable rigid devices enhancing biocompatibility and permitting signals (in the form of electrical impulses, ions, or molecules) to be sent on demand. We have shown that our synthetic neurons can perform simple electrochemical communication, albeit by a different mechanism to those employed by nature. Further, they can release transmitters that produce a downstream output (Fig. 3). Moreover, we have insulated the synthetic neurons and patterned them into nerve bundles, which can propagate distinct information simultaneously along parallel axons (Fig. 4). Our choice of soft materials ensures that our devices have structures and mechanics compatible with living tissues, including high flexibility to accommodate deformations arising from movement[3] (Fig. S22).

Our modular approach to the fabrication of synthetic nerves means that future devices can be scaled by adjusting axon dimensions, density, or number. In addition, the elements encapsulated within each sensory or presynaptic droplet can be varied. In this way, parallel axons might respond to different wavelengths of light[31] or different stimuli (e.g., various small molecules) and release different molecules (e.g., neurotransmitters or pharmaceuticals) on demand.

Whilst our synthetic neurons remained functional for at least a week after formation (when kept in a dark, hydrated chamber, Fig. S28), the device lifetime is yet to be fully explored. Further, in the current synthetic nerve design, prolonged illumination will eventually lead to the depletion of ions and molecules, limiting its longevity. In the future, nerve lifetime might be improved by including bioinspired elements such as a transmitter re-uptake system or perhaps synthesis machinery to generate the transmitter *in situ.* Additionally, future synthetic nerves should function within an aqueous environment. Previous droplet-based networks have been transferred from oil to water after coating the entire device in a thin hydrogel layer[44]. Alternatively, we suggest that transfer might be realised by incorporating the lipids into the elastomeric sheath allowing oil removal. Moreover, the inclusion of elements such as block co-polymers or emulsion stabilisers[45], might also be used to increase device robustness and prevent rupture when transferred to an aqueous environment.

We believe our soft, tetherless synthetic nerve is a valuable contribution to the development of next generation bioelectronics for applications in neurorobotics, neuro-prosthetics, computing, and medicine. For such applications, e.g., in the treatment of inflammation, the ability of the patterned device to locally and precisely administer treatment will be extremely advantageous. Further, a single device might both send and receive signals across the abiotic-biotic interface for healthcare monitoring and disease treatment.

Methods

Materials preparation. Microbial rhodopsins were gifted by the Anthony Watts Group, University of Oxford[30]. The final sensory droplets contained 0.15 - 0.25 mg mL^{-1} microbial rhodopsin protein (estimated from measurements taken with a Nanodrop 1000 spectrophotometer) in Solution A (100 mM MES, 100 mM NaCl, 0.001% DDM (w/v), pH 6.5). Microbial rhodopsins were stored at 4°C in the dark. Alpha-hemolysin (αHL) pore-forming monomers were gifted by Idil Cazimoglu (Bayley Group) and stored at -80°C. A fresh aliquot, containing 50 nM αHL (stock measured with the Nanodrop) in Solution B (100 mM MES, 100 mM NaCl, pH 6.5), was used for each experiment. Pyranine (100 µM, HPTS, ThermoFisher) was dissolved in Solution C (100 mM NaCl, pH 6.5) and stored at 4°C in the dark. Aliquots of ATP (Abcam, 100 µM) or MANT-dATP (Sigma, 100 µM) in Solution B containing αHL (50 nM) were stored at -20°C in the dark. Components of the ATP assay kit (Abcam, ab83355) were prepared and stored in line with the manufacturer's manual. Agarose (2% high-gelling agarose, Sigma) was dissolved in Solution B and stored at room temperature. Silicone elastomer monomer (SYLGARD 184, Sigma) and curing agent (Sigma) were stored at room temperature. The lipid-in-oil was 10 mg mL^{-1} DPhPC (Avanti 4ME 16:0 PC) in filtered (0.22 μm Millex GP filters, Millipore) hexadecane (Sigma) and silicone oil (AR20, Sigma) (35:65 (v/v)).

Electrical recording. Ag/AgCl electrodes were prepared from silver wire (100 µm diameter, Sigma) by incubating the tips in sodium hypochlorite (NaClO, 10% active chlorine, Sigma) and then applying an agarose coating (1% low-gelling, Sigma). The PMMA chamber, located within a Faraday cage, was filled with the lipid-in-oil and positioned directly below the fibre-coupled LED bundle. Droplets (200 nL, 700 µm diameter) were pipetted onto the electrodes (Finnpipette F1, 0.2-2 μL, ThermoFisher) and after a few minutes brought into contact to form a DIB, as confirmed by measurement of the capacitance (>20 pF) by application of a triangular voltage waveform ($\pm$15 mV, 30 s peak-to-peak, in the dark). The sensory droplet contained the recording electrode. Signals were recorded with an amplifier (Axopatch 200B), connected to a digitizer (Digidata 1440 A) and analysed using Clampfit (version 10.3) (Axon Instruments). A multichannel amplifier (Triton$^+$, Tecella LLC) was used for simultaneous recordings from the synthetic nerve (Fig. S25). Experiments were conducted at 24.5 $\pm$ 3.4°C and 32.4 $\pm$ 8.6% humidity.

Illumination source. A fibre carrying 7 separately controlled (using the manufacture's software (Mightex, WFC-H7-0560)) LEDs was used: UV light (LED 7): 367 nm, 15 $\pm$ 3.9 mW; IR light (LED 1): 722 nm 16 $\pm$ 5.0 mW; and YG light (LEDs 4 and 5 simultaneously): 592 nm and 550 nm, 15 $\pm$ 4.5 mW (Fig. S6).

Synthetic neuron construction. Droplet neurons were composed of a series of interconnected aqueous droplets (200 nL, ~700 µm diameter): sensory droplet (*S*), axon droplet(s) (*A*), presynaptic droplet (*Pre*) and postsynaptic droplet (*Pst*). For hydrogel neurons, an agarose fibre formed the axon (2% high-gelling agarose, 1-mm diameter, Fig. 1c). After droplet incubation (5 min in the lipid-in-oil to allow monolayer formation), the sensory and synaptic bilayers were formed by gently pushing into contact *S* and *A*, and *Pre* and *Pst* droplets, respectively. After a further 10- 20 min, the signalling pathway was completed. For overnight experiments, synthetic neurons were stored in a hydrated environment.

Synthetic nerve formation. Silicone elastomer monomer (SYLGARD 184, Sigma, 761036) and curing agent (Sigma, 761036) were mixed in a 10:1 (v/v) ratio and degassed for 30 min before being poured into a cast and placed in an incubator overnight at 60°C (Fig. S24). Once cooled, the elastomeric nerve structure was removed from the cast leaving seven tubular holes within it (1 mm diameter, 10 mm length). To form the conducting pathway, the holes were filled by pipetting hot 2% low-melt agarose in Solution B into them and then, after cooling, pre-incubated droplets (200 nL) were gently pushed into contact with the hydrogel axons.

Microscopy. Images were taken with a Leica DMi8 inverted epi-fluorescence microscope. Pyranine fluorescence was visualised at 5x magnification: excitation wavelength (λ_{ex}), 450-490 nm; emission wavelength (λ_{em}), 500-550 nm (Fig. 2, 4). MANT-dATP visualisation conditions were: 10x magnification and λ_{ex} 350-390 nm, λ_{em} 420-480 nm (Fig. 3c-d). Resorufin visualisation conditions were: 10x magnification, λ_{ex}, 540-552 nm, λ_{em}, 562-643 nm (Fig. 3e-f). Any brightness/contrast changes were the same within any image set.

Replicates. Each experiment had a minimum of three independent synthetic neurons/nerves.

Figure preparation. Brightfield photographs of the neurons (with food dyes) were background removed (using Microsoft PowerPoint, Fig. S29). Fluorescence images were stitched together to form one complete picture (using Fiji, ImageJ[46]). For pyranine images the background was then removed using a Fiji (ImageJ) mask (Fig. S30). Only the raw images were used for data processing and analysis (Fig. S30, S31).

References

1. Someya, T., Bao, Z. & Malliaras, G. The rise of plastic bioelectronics. *Nature* **540**, 379-385 (2016).
2. Choi, S., Han, S.I., Jung, D. *et. al.* Highly conductive, stretchable and biocompatible Ag-Au core-sheath nanowire composite for wearable and implantable bioelectronics. *Nat. Nanotech.* **13**, 1048-1056 (2018).
3. Lacour, S., Courtine, G. & Guck, J. Materials and technologies for soft implantable neuroprostheses. *Nat. Rev. Mater*. **1**, 16063 (2016).
4. Yang, X., Zhou, T., Zwang, T.J. *et. al.* Bioinspired neuron-like electronics. *Nat. Mater*. **18,** 510–517 (2019).
5. Kim, Y. Chortos, A., Xu, W. *et. al.* A bioinspired flexible organic artificial afferent nerve. *Science* **360**, 998-1003 (2018).
6. Wehner, M., Truby, R., Fitzgerland, D. *et. al.* An integrated design and fabrication strategy for entirely soft, autonomous robots. *Nature* **536**, 451–455 (2016).
7. Karbalaei Akbari, M., & Zhuiykov, S. A bioinspired optoelectronically engineered artificial neurorobotics device with sensorimotor functionalities. *Nat. Commun.* **10**, 3873 (2019).
8. Kuhnert, L., Agladze, K. I., & Krinsky, V.I. Image processing using light-sensitive chemical waves. *Nature* **337**, 244-247 (1989).
9. Gizynski, K., Gorecki, J. Chemical memory with states coded in light controlled oscillations of interacting Belousov-Zhabotinsky droplets. *Phys. Chem. Chem. Phys*. **19**, 6519-6531 (2017).
10. Parrilla-Gutierrez, J.M., Sharma, A. Tsuda, S. et. al. A programmable chemical computer with memory and pattern recognition. *Nat. Commun*. **11**, 1442 (2020).
11. Keene, S.T., Lubrana, C., Kazemzadeh, S. *et. al.* A biohybrid synapse with neurotransmitter-mediated plasticity. *Nat. Mater.* **19,** 969-973 (2020).
12. Van de Burgt, Y., Melians, A., Keene, S.T. *et. al.* Organic electronics for neuromorphic computing. *Nat. Electron.* **1**, 386-397 (2018).
13. Misra, N., Martinez, J.A., Huang, S-C.J. *et. al.* Bioelectronic silicon nanowire devices using functional membrane proteins. *Proc. Natl. Acad. Sci. USA* **106,** 13780-13784 (2009).
14. Amit, M., Roy, S., Deng, Y. *et. al.* Measuring proton currents of bioinspired materials with metallic contacts. *ACS Appl. Mater. Interfaces.* **10,** 1933-1938 (2018).
15. Lodish, H., Berk, A., Kaiser, C. *et. al.* Molecular Cell Biology (8th edition). (W.H. Freeman, 2016).
16. Pereda, A. Electrical synapses and their functional interactions with chemical synapses. *Nat. Rev. Neurosci*. **15**, 250-263 (2014).
17. Liu, Y., Liu, J., Chen, S. *et. al.* Soft and elastic hydrogel-based microelectronics for localized low-voltage neuromodulation. *Nat. Biomed. Eng.* **3**, 58–68 (2019).
18. Keplinger, C. Sun, J-Y., Foo, C.C *et. al.* Stretchable, transparent, ionic conductors. *Science* **341**, 984-987 (2013).
19. Yang, C., Suo, Z. Hydrogel ionotronics. *Nat Rev Mater* **3**, 125–142 (2018).
20. Owens, R.M., and Malliaras, G.G. (2010) Organic electronics at the interface with biology. MRS Bull. *35,* 449-456.
21. Strakosas, X., Bongo, M. & Owens, R. M. The organic electrochemical transistor for biological applications. *J. Appl. Polym. Sci.*, **132**, 41735 (2015).

22. Selberg, J., Gomez, M., & Rolandi, M. The potential for convergence between synthetic biology and bioelectronics. *Cell systems.* **7,** 231-244. (2018).
23. Villar, G., Graham, A.D., & Bayley, H. A tissue-like printed material. *Science* **340,** 48-52. (2013).
24. Booth, M.J., Restrepo Schild, V., Graham, A.D., *et.al*. Light-activated communication in synthetic tissues. *Sci Adv* e1600056, **2** (2016).
25. Holden, M.A., Needham, D., & Bayley, H. Functional bionetworks from nanoliter water droplets. *J. Am. Chem. Soc*. **129**, 8650-8655. (2007).
26. Restrepo Schild, V., Booth, M.J., Box, S. *et. al*. Light-patterned current generation in a droplet bilayer array. *Sci Rep* **7**, 46585 (2017).
27. Jones, G. King, P.H., Morgan, H., *et. al.* Autonomous droplet architectures. *Artif. Life*, **21**, 195-204 (2015).
28. Dupin, A., & Simmel, F.C. Signalling and differentiation in emulsion-based multi-compartmentalized in vitro gene circuits. *Nat. Chem.* **11**, 32-39 (2019).
29. Chow, B. Y., Han, X., Dobry, A. *et. al.* High-performance genetically targetable optical neural silencing by light-driven proton pumps. *Nature* **463**, 98–102 (2010).
30. Bada Juarez, J.F., Judge, P.J., Adam, S., *et. al.* Structures of the archaerhodopsin-3 transporter reveal that disordering of internal water networks underpins receptor sensitization. *Nat. Commun.* **12,** 629 (2021).
31. Ernst, O. P., Lodowski, D.T., Elstner, M. et. al. Microbial and animal rhodopsins: structures, functions and molecular mechanisms. *Chem. Rev*. **8**, 126-163 (2014).
32. Bamberg, E., Apell, H.J., Dencher, N.A., *et. al.* Photocurrents generated by bacteriorhodopsin on planar bilayer membranes. *Eur. Biophys. J.* **5**, 277–292 (1979).
33. Tunuguntla, R., Bangar, M., Kim, K. *et. al.* Lipid bilayer composition can influence the orientation of proteorhodopsin in artificial membranes. *Biophys. J.* **105**, 1388-1396 (2013).
34. Inoue, K., Tsukamoto, T., Shimono, K. *et. al.* Converting a light-driven proton pump into a light-gated proton channel. *J. Am. Chem. Soc*. **137**, 3291-3299 (2015).
35. Huang, K-S., Bayley, H., & Khorana, H.G. Delipidation of bacteriorhodopsin and reconstitution with exogenous phospholipid. *Proc. Nat. Acad. Sci. USA* **77,** 323-327. (1980).
36. Ming, M., Lu, M., Balashov, S.P. *et. al.* pH dependence of light-driven proton pumping by an archaerhodopsin from Tibet: comparison with bacteriorhodopsin. *Biophys. J.* **90**, 3322-3332. (2006).
37. Bean, B. The action potential in mammalian central neurons. *Nat. Rev. Neurosci*. **8**, 451–465 (2007).
38. Yanoff, M., & Sassani, J.W. '13 - Optic Nerve' in *Ocular Pathology (8th edition) pg.* 494 (Elsevier, 2020).
39. Burnstock, G. Historical review: ATP as a neurotransmitter. *Trends Pharmacol. Sci*. **27**(3), 166-176 (2006).
40. Soto, E., Ortega-Ramírez, A., & Vega, R. Protons as messengers of intercellular communication in the nervous system. *Front. Cell. Neurosci*. **12**, 342. (2018).
41. Du, J., Hossain, Z., & Mandal, J. Protons: a neurotransmitter in the brain. *Edorium J Cell Biol*. **3**, 1-3 (2017).

42. Guerra-Gomes, S., Sousa, N., Pinto, L., & Oliveira, J.F. Functional roles of astrocyte calcium elevations: from synapses to behaviour. *Front. Cell. Neurosci.* **11**, 427 (2018).
43. Yoshimura, K., Kouyama, T. Structural role of bacterioruberin in the trimeric structure of archearhodopsin-2. *J. Mol. Biol*. **375**, 1267-1281 (2008).
44. Graham, A. D., Olof, S.N., Burke, M.J. *et. al.* High-resolution patterned cellular constructs by droplet-based 3D printing. *Sci Rep*. **7,** 7004 (2017).
45. Jeong, D-W., Jang, H., Choi, S., & et. al. Enhanced stability of freestanding lipid bilayer and its stability criteria. *Sci. Rep.* **6,** 38158 (2016).
46. Preibisch, S., Saalfeld, S., & Tomancak, P. Globally optimal stitching of tiled 3D microscopic image acquisitions. *Bioinformatics.* **25**(11), 1463-1465 (2009).

Acknowledgements

Work in the H.B. group is supported by a European Research Council Advanced Grant (SYNTISU). C.E.G.H. was supported by Oxford's Centre for Doctoral Training in Synthetic Biology, which is funded by the University of Oxford, the Engineering and Physical Sciences Research Council (EPSRC) and the Biotechnology and Biological Sciences Research Council (BBSRC) (EP/L016494/1). Microbial rhodopsins were a gift from the Anthony Watts Group (Department of Biochemistry, University of Oxford) and α-hemolysin the gift of Idil Cazimoglu (Bayley Group, University of Oxford). We thank Dr David Lunn for discussions regarding the use of elastomers. We also thank Al Walter and Yoke Tanaka (Tecella) for their assistance.

Author Contributions

C.E.G.H., V.R.S., and H.B. conceived the ideas behind the project, discussed the data and wrote the manuscript. C.E.G.H. (with assistance from V.R.S.) carried out the experiments and analysed the data. J.V.C. prepared the microbial rhodopsins.